RESEARCH PAPER

Acid treatment of melanoma cells selects for invasive phenotypes

Raymond E. Moellering · Kvar C. Black · Chetan Krishnamurty ·
Brenda K. Baggett · Phillip Stafford · Matthew Rain · Robert A. Gatenby ·
Robert J. Gillies

Abstract Solid tumors become acidic due to hypoxia and upregulated glycolysis. We have hypothesized that this acidosis leads to more aggressive invasive behavior during carcinogenesis (Nature Reviews Cancer 4:891–899, 2004). Previous work on this subject has shown mixed results. While some have observed an induction of metastasis and invasion with acid treatments, others have not. To investigate this, human melanoma cells were acclimated to low pH growth conditions. Significant cell mortality occurred during acclimation, suggesting that acidosis selected for resistant phenotypes. Cells maintained under acidic conditions exhibited a greater range of motility, a reduced capacity to form flank tumors in SCID mice and did not invade more rapidly in vitro, compared to non-selected control cells. However, re-acclimation of these selected cells to physiological pH gave rise to stable populations with significantly higher in vitro invasion. These re-acclimated cells maintained higher invasion and higher motility for multiple generations. Transcriptomic analyses of these three phenotypes revealed significant differences, including upregulation of relevant pathways important for tissue remodeling, cell cycle control and proliferation. These results reinforce the hypothesis that acidosis promotes selection of stable, more invasive phenotypes, rather than inductive changes, which would be reversible.

R. E. Moellering · K. C. Black · C. Krishnamurty ·
B. K. Baggett · R. J. Gillies
Arizona Cancer Center, Arizona Health Sciences Center,
Tucson, USA

Present Address:
R. E. Moellering
Department of Chemistry and Chemical Biology, Harvard
University, 12 Oxford Street, Cambridge, MA 02138, USA

P. Stafford
Translational Genomics Research Institute (TGen),
445 N. 5th St, Phoenix, AZ 85004, USA

M. Rain
Agilent Technologies, 5301 Stevens Creek Blvd, Santa Clara,
CA 95051, USA

R. A. Gatenby · R. J. Gillies (✉)
Department of Radiology, Arizona Cancer Center,
1515 N Campbell Ave, Tucson, AZ 85724-5024, USA
e-mail: gillies@u.arizona.edu

Keywords Acid–base · Melanoma · Evolution · Invasion · Motility

Abbreviations

DMEM	Dulbecco's Modified Eagle's Medium
MAPK	Mitogen-activated protein kinase
MMP	Matrix metalloproteinase

Introduction

Progression of carcinogenesis is influenced by microenvironmental and metabolic systems at work in pre-malignant lesions [1]. Because in situ epithelial tumors develop in an avascular environment, they are exposed to hypoxic microenvironments that select for profoundly different metabolic phenotypes that are able to survive and proliferate under these harsh conditions [2–4]. Adaptation to hypoxia leads to transcriptional activation of genes involved in glycolysis and recent data suggest that hypoxia

and the subsequent up-regulation of the glycolytic phenotype is an early event in carcinogenesis [5]. Consequently, these glycolytic phenotypes lead to acidification of the extracellular space due to increased metabolic flux combined with poor perfusion [6]. In most cancers, increased metabolic acid production is accompanied by up-regulation of proton-exporting systems, such as $H^+/ATPase$ and H^+/Na^+ exchangers and combined, these effects lead to extracellular acidosis, with pH values commonly seen in the range of pH 6.5–6.7 [7]. Survival of tumor cells in this acidic environment depends on down-regulation of pro-apoptotic machinery and/or up-regulating proton exporting transporters [8–11].

The environment created by these resistant phenotypes serves as an adaptive advantage because they create an environment that is toxic to native populations yet harmless to themselves [12]. In addition, acidosis promotes excretion of numerous proteolytic enzymes that are involved in tissue remodeling [13]. One class of membrane remodeling enzymes believed to be crucial for invasion is matrix-metalloproteinases (MMPs), a family currently including at least 22 members [14]. Although MMPs exhibit alkaline pH optima, low pH has been shown to increase their activation and release [13, 15]. Furthermore, enzymes such as cathepsins and urokinase-like plasminogen activator (uPA) often show increased secretion and activity in tumors [16–18]. Hence, these key proteolytic systems in tumor invasion are linked by expression, secretion and activation to microenvironmental acidosis, although the precise mechanisms for this activation have not been elucidated. Activation of proteases may promote degradation of the basement membrane allowing escape of tumor cells into the vasculature, or metastasis, thus converting an in situ cancer to one that is invasive [19].

To date, most studies investigating the microenvironmental effects on invasion and metastasis have assumed that low pH induces the measured phenotypes or behaviors [15, 20, 21]. For example, pre-treatment of melanoma cells with acid conditions for as little as 24 h increases their ability to form metastases following tail vein injection [20, 22]. However, it is not known whether the effects on motility and invasion are merely the sum of numerous inductive fluctuations stemming from acidosis, or if the cells exhibiting the metastatic phenotype are discretely selected populations. Such a distinction would be important in the context of understanding carcinogenesis and progression. The current study investigates this by monitoring the effect of acidosis on the invasive, motile, and tumorigenic behavior of human melanoma cells and results indicate that acidosis selects for, rather than induces, an invasive phenotype. Subsequently, it was shown that these phenotypes were associated with altered expression of genes relevant to tissue remodeling and apoptosis. Thus, in this system, low pH selects for

phenotypes that are more invasive, and this occurs through a surprisingly stable increase in the phenotypic diversity as well as global changes in mRNA expression profiles.

Materials and methods

Cell culture

Human melanoma (C8161) cells were obtained from the Arizona Cancer Center Shared Service and cultured in Dulbecco's Modified Eagle's Medium (DMEM)/Ham's Nutrient Mixture F-12 (Sigma, St. Louis, MO), with 10% Fetal Bovine Serum in a 5% CO_2 atmosphere at 37°C. Media was further supplemented with 20 mM each HEPES, MES and MOPS buffers, and 14.2 mM sodium bicarbonate. Media did not contain phenol red for compatibility with fluorescent invasion assays. Media pH was adjusted to either 7.4 or 6.7. Cells were grown in T-25 flasks and passed approximately once a week at confluence.

Generation of low pH and C8161/LH-1 phenotypes

Acclimation of cells at pH 7.4 to 6.7 was a slow conditioning process over the course of 1.5 months. This was accomplished by lowering the media pH systematically by approximately 0.15 pH units every two weeks with cultures being passed twice between rounds of further acidification. The low pH (6.7) acclimated cultures (C8161/6.7) were maintained at pH 6.7 for one month before an aliquot of cells were reintroduced to normal (7.4) pH, creating the C8161/LH (also named C8161/LH-1) cell line. Later reintroduction of low pH phenotype to pH 7.4 generated subsequent C8161/LH-1 lines, denoted as C8161/LH-2, which were maintained at low pH for two months prior to re-acclimation at normal pH; and C8161/LH-3, which were maintained at low pH for three months before re-acclimation. Native C8161 cells were cultured continuously at pH 7.4, and were denoted as C8161/7.4 cells.

Cell viability and colony formation

Cell growth curves were counted via a Coulter counter in quadruplicate per well. Cell viability and colony formation were determined by crystal violet staining. Cells were plated at pH 7.4 overnight, wells were washed once with pH 6.7 media and fresh 6.7 media was added to the wells. At the appropriate time points, wells were washed once with pH 7.4 media, then fresh 7.4 media was added for recovery. For the kill curve data, cells were allowed to recover in media at pH 7.4 for 16 h prior to crystal violet

staining. For colony formation assays, cells were allowed to recover at a pH of 7.4 for 1 week prior to crystal violet staining. For staining, cells were fixed with 0.025% gluteraldehyde for 30 min, stained with 0.1% crystal violet for 60 min, destained with water for 60 min and allowed to fully dry. For cell viability, 1% acetic acid was added to solubilize crystal violet stained cells, and absorbance was read at a wavelength of 590 nm. Colony formation assay was achieved by staining, then visually counting the colonies that formed from viable cells.

Fluorescent cell labeling

The lipophilic fluorescent dye DiO-C_{18} was obtained from Molecular Probes (Eugene, OR). A stock solution was created by dissolving 7.5 mg solid DiO in 5 ml dimethyl formamide, followed by sonication at 50°C for 10–15 min. This solution was stored at 4°C away from light. Suspension labeling was carried out after trypsinization of confluent cultures and resuspension of cells in 3 ml of media containing 5% FBS. 15 μl DiO stock was added to this suspension followed by mild shaking (50 rpm) and incubation at 37°C for 40 min. Following incubation, suspensions were centrifuged at 1000 rpm for three minutes and supernatant removed. Pellet was again suspended in 3 ml media, centrifuged, supernatant was removed, and finally suspended in DMEM of appropriate pH containing 0% FBS.

Real-time transwell invasion assay

24-well Tumor Invasion System Plates containing Matrigel^{TM} inserts were obtained from BD-Biosciences (Bedford, MA). Plates were stored at −20°C and warmed to room temperature prior to use. DiO labeled cells were seeded at 65,000 cells in 300 μl serum-free media in the upper well. Each condition was seeded in quadruplicate and 500 μl of media containing 5% FBS of the corresponding pH was placed into lower wells of the plate. One column of wells held a serial dilution ranging from 20,000 to 80,000 cells seeded in the bottom well for generation of a standard curve.

Epi-fluorescence measurements were made using the Victor-3 Multi-Label plate reader (Wallac/PerkinElmer, Finland) with excitation at 485 nm and emission at 510 nm. Plates were incubated at 37°C in 5% CO_2 and measurements were taken every six to eight hours over a period of 48 h. After the final time point, media from top and bottom wells were aspirated, cells and Matrigel were removed from the top of the well, and cells were washed once with 400 μl of phosphate buffered saline (PBS) followed by 400 μl trypsin. Trypsinization was carried out at 37°C with shaking at 40 rpm for 10 min to remove invasive cells from the underside of the Matrigel insert. The trypsinized cell suspension was aspirated and added to 1 ml of media containing 10% FBS. This process was repeated once more to ensure thorough removal of all invasive cells. A ratio of 0.1597 ± 0.003 was observed in the fluorescence of cells adhering to filter, compared to cells at the bottom of the well. Final cell suspensions were counted twice using a hemacytometer and averaged to represent the number of invading cells per well, as needed for the calibration of the fluorescence data. Over the range of interest, fluorescence was linear with cell number and invasion was linear with time over the 48 h investigation. A linear equation was generated and applied to each time point translating fluorescence into invasive cell number.

Motility assay

Motility was monitored with time-lapse cinematography using cells cultured in a thermostatic sealed microscope chamber, according to manufacturer's specifications (model FCS2®, Bioptechs, Butler, PA). Briefly, a silica glass coverslip was placed in a non-cell culture Petri dish, and 5×10^5 cells were added to the dish containing 10 ml of the same stock solution of DMEM/F-12 described above, equilibrated to the proper pH. The dish was incubated for two days to assure cell adherence and viability on the coverslip. After incubation, the coverslip was placed in a closed cell chamber that allowed for perfusion of media during experimentation. Temperature of the chamber was equilibrated to 37°C with temperature objective heater and controller. The chamber was placed on an Olympus IMT-2 inverted microscope (Olympus, Melville, NY) and imaged using Differential Interference Contrast (DIC)/Nomarski acquisition. The magnification of the microscope was set to 10×1.5. A field containing 10–25 viable cells was identified, and time-lapse videography was performed on the cells using a digital camera (Hamamatsu, 640 by 512 pixels) attached to the microscope, linked to a computer running SimplePCI software (C-Imaging Systems, Compix Inc., Sewickley, PA). The image capture rate was one frame/min. Warmed media was perfused through the chamber at a rate of 100 μl/h. Images were captured over six hours.

Motility was quantified using a cell-tracking software tool, described below. A region of interest (ROI), usually the cell nucleus, was tracked over the first hour of the time-lapse experiments. The tracking process was displayed on screen to facilitate the user in monitoring the movement of the original ROI from one frame to the next.

Cell tracking software tool

A cell-tracking tool was developed using IDL 6.0 (Research Systems, Inc., Boulder, CO). This tool allowed the user to define the ROI (cell) boundary by selecting points using a mouse. The user-defined ROI boundary (contour) was used as the initialization for tracking process. The ROI boundaries on the following frames were detected using a combination of block matching and the gradient vector flow (GVF) snake [23]. The tool quantified the inter-frame displacement of the centroid of the ROI. It also allowed for automation of the process by quantifying five frames at a time, while displaying the location of the ROI in each frame. Manual editing of the ROI at any time by the user was available if the user determined that the program has failed to track the cell boundary accurately. The user interface showed dynamic values of interframe displacement and total displacement (in microns and pixels) during quantification, and generated values of average velocity (sum of inter-frame displacements divided by total time, in microns/min and pixels/min), total displacement, and net displacement (distance between original and final ROIs) at the end of the tracking process.

Expression array processing and analysis

Agilent Whole Human Genome Expression arrays (Agilent Technologies, Palo Alto, CA) were run as dye flips in triplicate, accommodating technical labeling variance only, according to the manufacturer's protocol. Cells were processed for RNA using Ambion's Quick-Extract system and RNA Ladder (http://www.ambion.com). 50 ng of RNA from each of the cell lines (C8161/6.7, C8161/7.4, and C8161/LH) were labeled with CY3 and CY5. Each species of labeled cRNA was applied to each of three replicate arrays, for a total of eighteen arrays covering each species on each channel three times. Data were analyzed in GeneSpring 7.2 (Agilent Technologies, Palo Alto, CA). Images and output from Feature Extraction version 7 (Agilent Technologies, Palo Alto, CA) were consistent with high-quality data [24]. Dye flips were mathematically inverted, but the labels remained as originally hybridized for the figures. Data from each two color array were expressed as a direct compared ratio (i.e. C8161/7.4:/LH, /6.7:/LH, /6.7:/7.4) and these were each replicated six times for a total of eighteen arrays. /7.4:/LH refers to a two-channel slide where C8161/7.4 cells labeled with CY5 were hybridized against CY3-labeled C8161/LH-1 cells. Comparison between phenotypes used ratios with a common denominator. Hence, comparing C8161/6.7 cells to C8161/7.4 cells compared the /6.7:/LH and /7.4:/LH ratios, etc. Single-color data were examined and were consistent with ratio data where applicable. Only ratio data are presented here. Expression data were analyzed using a homoskedastic Fixed Effects (Model I) One-Way ANOVA for three-way comparison and Student's t-test with a threshold of $P < 10^{-8}$ for individual tests, multivariate analyses (hierarchical clustering, Principal Components Analysis) and functional tests (Gene Ontology Binomial Test). Tests against GenMapp, Biocarta and KeGG were done through the Biorag (http://www.biorag.org) interface at the Arizona Cancer Center, Tucson, AZ (http://www.azcc.arizona.edu).

Quantitative RT-PCR

RNA samples from 1×10^6 cells of each phenotype were prepared using an RNEasy Mini kit (Qiagen, Valencia, CA). Total RNA was reverse transcribed to cDNA using SuperScript II Reverse Transcriptase Kit according to the manufacturer's protocol (Invitrogen, Carlsbad, CA). The resulting cDNA was used as the substrate to measure gene expression levels by qPCR with TaqMan probes and primers specific for HEY1 (Probe ID: Hs00232618_m1), SNAI1 (Probe ID: Hs00195591_m1) and β-Actin (Probe ID: 4352935E). Triplicate reactions were prepared in 384-well optical PCR plates (Applied Biosystems, Foster City, CA) with 10 μl 2× TaqMan DNA Polymerase mastermix (Applied Biosystems, Foster City, CA), 1 μl TaqMan probe/primer mastermix and 9 μl of cDNA diluted in nuclease-free water. qPCR was performed using a ABI Prism 7900 (Applied Biosystems, Foster City, CA) instrument with the following run specifications: FAM probe detection, AmpErase activation for 2 min at 50°C, DNA polymerase activation for 10 min at 95°C followed by 40 cycles of duplex melting for 15 s at 95°C and annealing for 1 minute at 60°C. Threshold cycle (Ct) values were automatically calculated within the instrument software for each replicate and used to determine the fold change for each gene/phenotype set relative to C8161/7.4 cells by the following formulas:

$$\Delta Ct = Ct(GOI) - Ct(BA)$$

where Ct(GOI) is the Ct value for the gene of interest and Ct(BA) is the Ct value for β-Actin.

$$\Delta\Delta Ct = \Delta Ct(\text{phenotype C8161/6.7 or LH}) - \Delta Ct \\ (\text{phenotype C8161/7.4}).$$

Fold Change = $2^{\wedge}(-\Delta\Delta Ct)$ for each gene/phenotype combination relative to the C8161/7.4 cells.

Results

Acidic selection of melanoma cells

Early efforts were focused on acclimating melanoma cells to pH levels commonly found in the tumor microenvironment.

As described in *Materials and methods*, this process required approximately 1.5 months and was accompanied by substantial cell death with each decrease in pH. Empirically, cell death during the acclimation process appeared to be the natural response of the population to a toxic environment and selection of resistant phenotypes. Figure 1a shows a kill curve of parental (native) cells exposed to pH 6.7 over a time course of 48 h. Colony formation (Fig. 1 insets) assays demonstrated a 40–50% decrease in colony number after 48 h exposure to pH 6.7. After the full acclimation process, the new low pH population (C8161/6.7) grew slower than the parental at normal pH (C8161/7.4) cells when tested at the respective growth pH values (Fig. 1b). Doubling times are shown in Table 1, which also indicates the relative number of cells expected at 45 h, using the equation; $N = N_0(2^{45/\alpha})$, where α is the doubling time, in hr. Notably, when tested at pH 7.4, the growth rates of C8161/7.4 and C8161/6.7 cells were indistinguishable (Fig. 1c). Morphologically, C8161/6.7 and C8161/7.4 cells were markedly different (Fig. 2a–c). Compared to the C8161/7.4 cells, C8161/6.7 cells were heavy vacuolated, larger, and had sinuous, ragged filipodia. By morphology alone, these cells appeared to be under environmental stress.

The kill curve (Fig. 1a) suggests that acclimation of cells to low pH is a selection process, rather than a simple change in gene expression patterns. To investigate this, after 1–3 months at low pH, aliquots of the low pH cells

Table 1 Doubling times of pH phenotypes (hr ± SEM)

Test pH	Phenotype		
	7.4	7.4 → 6.7	7.4 → 6.7 → 7.4 (LH)
6.7	n/a	36.2 ± 2.6	n/a
7.4	23.4 ± 2.0	24.3 ± 2.2	23.7 ± 1.6
Cell number @ 45 hr (corr fact)	6.84	3.46 @ 6.7 6.24 @ 7.4	6.67

were re-acclimated to normal pH, generating the C8161/LH phenotypes (defined in the Materials and methods). This occurred without noticeable cell death, suggesting the absence of reselection. Notably, although the C8161/LH-1 phenotype had the same pH environment as the C8161/7.4 cells, they retained the morphology of the C8161/6.7 phenotype. Although they were not as ragged as C8161/6.7 cells, the C8161/LH-1 cells were larger, more vacuolated and had more filipodia than the parental C8161/7.4 phenotype (Fig. 2c).

Quantitative phenotyping of invasive potential

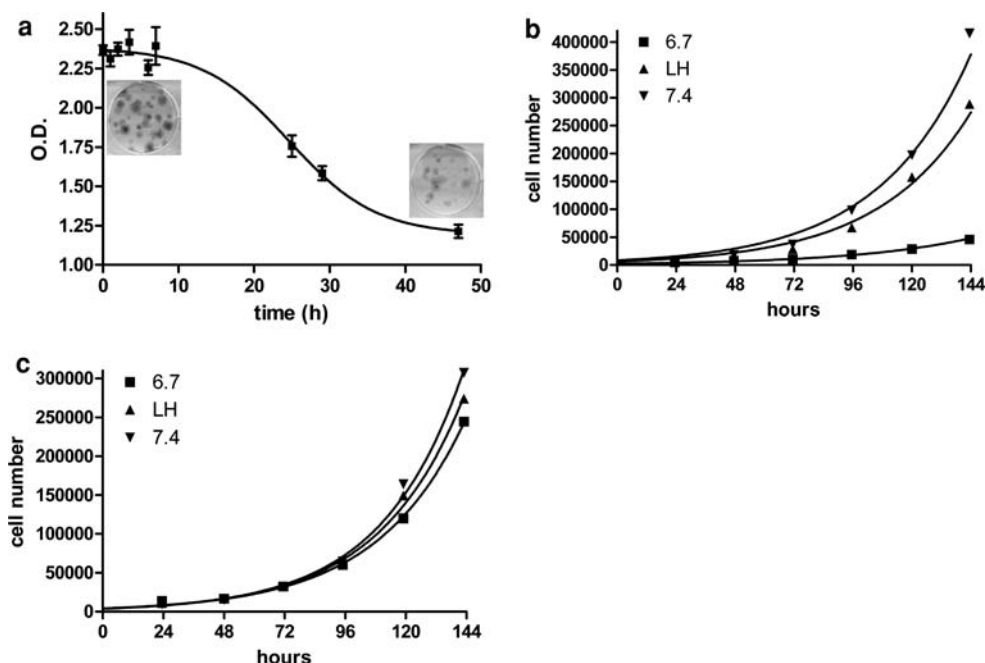One of the key events in metastasis is invasion of the neoplastic cells through the basement membrane. To

Fig. 1 Effects of pH on growth and survival. (**a**) Kill curve determined by crystal violet staining of parental C8161/7.4 cells exposed to pH of 6.7 for various lengths of time. Insets are corresponding colony formation assays after 0 and 48 hours exposure to pH 6.7. (**b**) Growth curve of cell phenotypes maintained in media matched to the pH phenotype: i.e. pH 6.7 for C8161/6.7; pH 7.4 for C8161/7.4 and C8161/LH demonstrates that the C8161/6.7 cells grew slower than the parental cell line, C8161/7.4 and the reacclimated cell line C8161/LH. (**c**) Growth curve of cell phenotypes, assayed in pH 7.4 media, showing that the growth rate of the three phenotypes were similar when grown at physiological pH
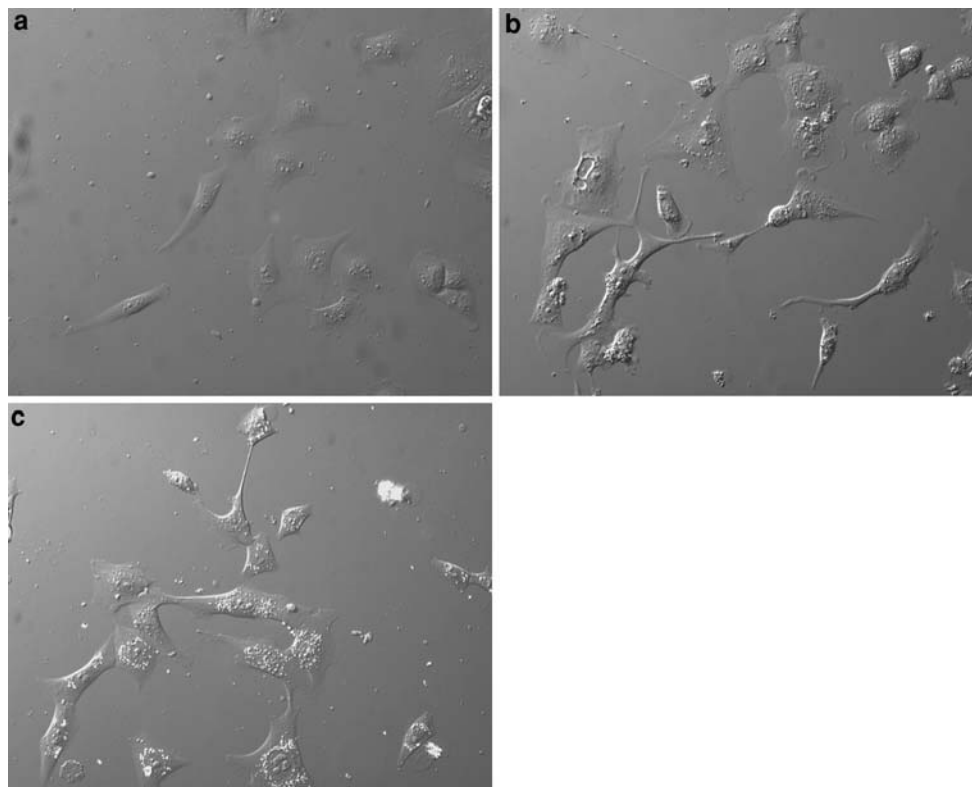
Fig. 2 Morphological effects of acidic selection. These images were captured during time-lapse analysis of motility, as described in Materials and Methods. (**a**) Native phenotype of C8161/7.4 cells grown and imaged at pH 7.4 shows mostly rounded cells with relatively smooth filipodia. (**b**) C8161/6.7 cells grown at pH 6.7 for two months and imaged at pH 6.7 were vacuolated with many jagged filipodia. (**c**) C8161/LH-1 cells were imaged one month after re-acclimation at pH 7.4 remain heavily vacuolated, similar to the low pH phenotype.

investigate this process in vitro, cells were fluorescently labeled and quantified as they invaded through a Matrigel^{TM} matrix, allowing for direct measurement of invasive potential. Labeling of cells with DiO-C$_{18}$ resulted in diffuse membrane staining with some punctuate fluorescence, indicating some internalization (Fig. 3a). Fluorescent images of the Matrigel membranes after a 24-h incubation period revealed a robust fluorescent signal from the invasive cells (Fig. 3b, c). These images qualitatively show the difference between phenotypes with different invasive potentials. Notably, the precision is high, due to low background fluorescence (Fig. 3d). The time-dependent behavior of this system is shown in Fig. 4a, which shows a linear increase in fluorescence on the lower side of the transwell membrane as a function of time. For comparison, 50,000 labeled cells were inoculated into the lower well and the fluorescence remained constant throughout the course of the assay. These data allow for the conversion of a fluorescent signal to the number of invading cells over the course of 2–3 days of incubation.

Results from this assay revealed robust quantitative differences in the invasive potential of the C8161/6.7, C8161/7.4, and C8161/LH-1 cells. These data are presented in Table 2 and Fig. 4b and show that cells conditioned to and tested at a pH of 6.7 appeared to have a slightly decreased potential to invade the barrier relative to C8161/7.4 cells cultured and tested at pH 7.4. Using uncorrected raw fluorescence, invasion of these low pH cells was $39 \pm 9\%$ that of the parental C8161/7.4 cells ($P < 0.001$). However, since the dye tracking will be diluted with cell proliferation, the amount of dye per cell may be lower at the end of the experiment, compared to the beginning. To compensate for this, dye values were also "corrected" using the expected differences in cell numbers from Table 1. After this correction, the difference in cell invasion was still less, at $77 \pm 18\%$ ($P < 0.01$), compared to that of the parental cells. With or without the correction factor, the C8161/6.7 cells re-cultured at pH 7.4 (the C8161/LH-1 phenotype) exhibited a significant ($P < 0.005$) increase in invasion compared to the C8161/7.4 cells. These results strongly suggest that acidic treatment of C8161 cells resulted in an upregulation of invasive properties. These experiments were repeated with these same cells over the course of four months in four separate assays, which consistently showed increased invasion of the C8161/LH-1 cells, indicating that the phenotypes were
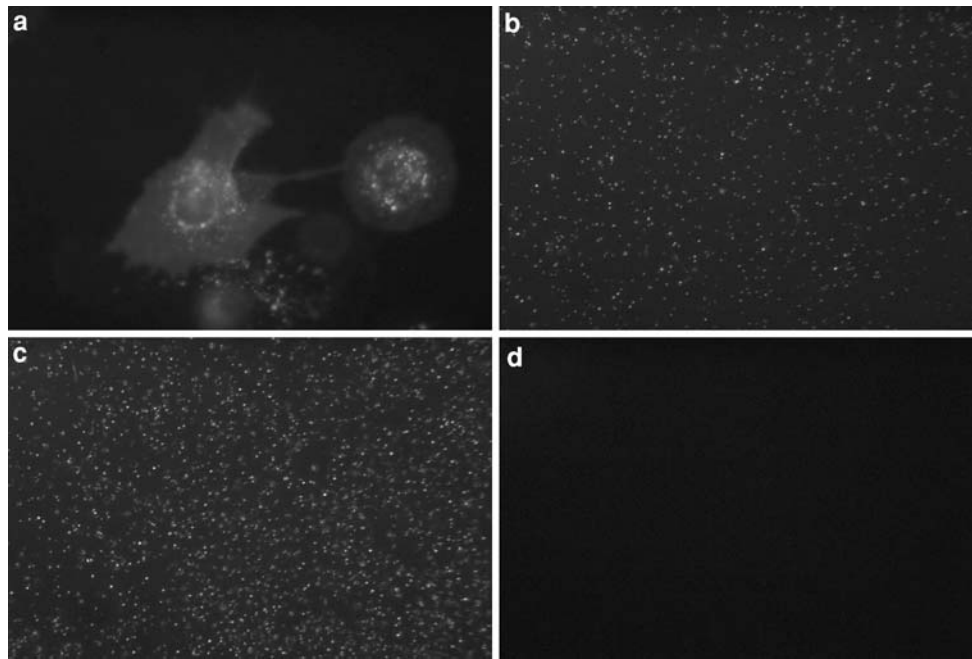
Fig. 3 Fluorescence imaging of invading cells. (**a**) C8161/7.4 cells were imaged at 100× following incubation with Di-O CellTracker[TM] dye, demonstrating even dye distribution throughout the membrane with some internalization. The under side of transwells were imaged after 24 h of invasion of (**b**) C8161/6.7 and (**c**) C8161/7.4 cells, showing higher invasion in the /7.4 compared to the /6.7 cells, (**d**) shows a transwell at initiation of assay using C8161/7.4 cells (i.e. 0 h of invasion), showing that cell fluorescence was efficiently blocked by the FluroBloc® membrane.

stable (Table 2). Furthermore, the time dependence of the re-acclimation process was explored by assaying C8161/LH lines generated one, two and three months after creation of the low pH phenotype (C8161/LH-1, /LH-2 and /LH-3, respectively). All C8161/LH lines exhibited increased invasion in each experiment. Although the /LH-2 and /LH-3 cell lines were significantly higher than parental C8161/7.4 cells ($P < 0.01$), they were also slightly, but significantly, less invasive than C8161/LH-1 cells ($P < 0.05$).

Cellular motility

While invasion assays quantified population averages with regard to invasive potential, in vitro motility assays were used to quantify movement of individual cells over time. Since no chemoattractant was used, and therefore no directed motion was expected, random motion average velocity of each cell was quantified by summing all the interframe displacements, as described in *Materials and methods*. The distribution of average velocities for all cells, separated into each environmental condition is shown in Fig. 5a. No statistically significant differences in average field velocity were seen among any of the phenotypes. However, other differences between cell population motility became evident upon further analysis.

The cell distributions clearly show extreme high and low velocity for both the C8161/6.7 and C8161/LH-1 phenotypes. Figure 5b and c show higher standard deviations and overall range of velocities for C8161/6.7 and C8161/LH-1 cells, compared to parental C8161/7.4 cells. Motility of the C8161/LH-1 and C8161/6.7 cells also showed an increased variance, which can be appreciated from the distribution histograms (Fig. 5d–f). In these plots, individual cell velocities are plotted and results from four to five independent experiments are overlaid. It can be seen from these graphs that both the C8161/LH-1 and C8161/6.7 phenotypes had substantial populations of cells with very high velocities (>0.8 μm min^{-1}), whereas only one of the C8161/7.4 cells showed this high velocity during the course of four experiments. By rank-ordering, 4% and 10% of the C8161/6.7 and C8161/LH-1 cells, respectively, were faster than all of the C8161/7.4 cells.

Tumorigenecity of acid selected phenotypes

Coupled with the potential to invade the basement membrane in metastasis, the ability to recruit nutrients, blood supply, and ultimately form tumors is an important aspect of cancer progression. To explore the tumorigenic potential of these melanoma phenotypes, SCID mice were inoculated with flank tumors and growth was monitored.
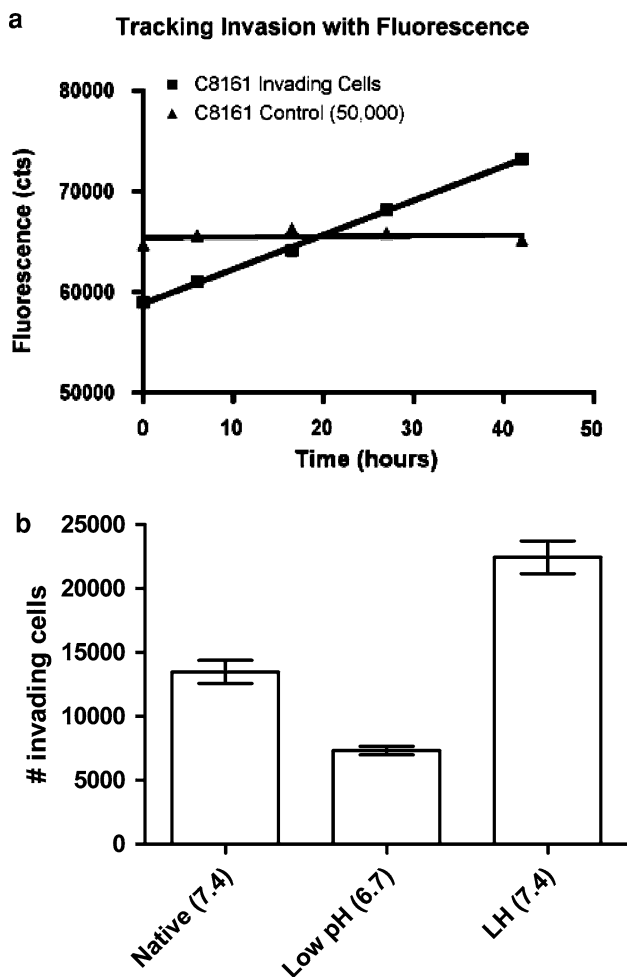
a Tracking Invasion with Fluorescence

■ C8161 Invading Cells
▲ C8161 Control (50,000)

b

Fig. 4 Quantitative fluorescent tracking of invasion. (**a**) Invasion curve using DiO labeled C8161/7.4 cells with transwell invasion assay. Cells were seeded in the lower well of the apparatus mimicking cells post-invasion (triangles). Signal remained constant over a 42-h incubation period showing that fluorescence was not affected by cell proliferation or fluorophore quenching. The invasion curve (closed squares) shows output signal from an equal number of cells seeded in the top chamber of the invasion apparatus at t = 0. Fluorescence increase was linear with time ($r^2 = 0.99$). (**b**) Representative invasion assay results for C8161 phenotype lines assayed in their respective media. After 45-h incubation, the numbers of invading cells were 48% and 160% for the C8161/6.7 and C8161/LH cell lines, respectively, relative to the parental C8161/7.4 cells

Figure 6 shows that both the C8161/LH phenotype and C8161/7.4 phenotypes exhibited similar growth. The C8161/LH-1 phenotype produced significantly larger tumors after two weeks ($P = 0.015$) and three weeks ($P = 0.048$), which was probably due to a decreased lag-time for tumor initiation and growth. Interestingly, the C8161/6.7 cells did not appear to have any in vivo tumorigenic capacity over this time-period. Instead these cells were stagnant for approximately 42 days before any noticeable growth was observed, clearly showing a significantly increased lag-time compared to the C8161/7.4

**Table 2** Invasion (relative to parental 7.4 cells)

Phenotype		% Invasion (uncorrected/corrected) at:				
		1 month	2 months	3 months	4 months	average
6.7	Uncorr	35	52	38	31	39 ± 9
	Corr	69	103	75	61	77 ± 18
LH-1	Uncorr	137	160	144	156	149 ± 11
	Corr	140	164	148	160	153 ± 11
LH-2	Uncorr		120	113		117 ± 5
	Corr		123	116		120 ± 5
LH-3	Uncorr			121		121
	Corr			124		124

and C8161/LH-1 tumors. These results were interpreted to indicate that the C8161/6.7 cells were more fragile and hence, had a lower surviving inocula, compared to the other cells. This would suggest that cells in an acidic environment must require a period of re-acclimation to physiological pH before they can successfully colonize. In addition, cells from the C8161/6.7 tumors of these SCID mice were isolated and recultured under both pH 6.7 and 7.4 conditions and then re-injected into SCID mice. These tumors developed from these cells continued to demonstrate a similar lag time as the original C8161/6.7 cells (Fig. 6). Eventually, the C8161/6.7 tumors grew at a rate comparable to the C8161/7.4 and C8161/LH-1 cell lines.

Transcriptome results

The above data indicate that selection by low pH generates a distinct and stable phenotype. In order to begin identifying the gene expression patterns associated with this phenotypic switch, RNA was extracted from each of the cell lines under their respective pH conditions and analyzed with Agilent genome arrays, as described in *Materials and methods*. The top 500 genes per category and the respective overlaps between data sets are shown in Fig. 7c. Notably, a subset of 40 genes was identified as being significantly altered (up- or down-regulated) among all cell lines using the individual T-tests and the ANOVA across all conditions. Each of these lists was analyzed further for functional significance using the Gene Ontology database (Table 3) and the biological databases Biocarta, GenMapp, and KeGG (Table 4). The three T-test lists, the ANOVA list, a supervised 423-gene cancer list, and a list of 500 random genes were included in each analysis. Each of the gene lists is graphically shown in Fig. 7a–c, where green represents underexpression and red represents overexpression. The identifier for each of these graphs describes in shorthand the data that were used for the t-test or the ANOVA significance test: e.g. LH vs. 6.7 describes the

Fig. 5 Heterogeneity of motility among phenotypes. The average velocity of individual cells was explored using the motility assay and cell-tracking software described in Materials and Methods. Figures (**a–c**) show histograms of 4–5 separate experiments per cell line wherein motility was tracked and velocities obtained from single cells. Results from different experiments are shown with different bar fill patterns. (**d–f**) show results of histogram analyses. No significant difference in the field average velocity was observed between the melanoma cell phenotypes (**a**), but the low pH and LH phenotypes exhibited a much wider cellular motility distributions (**b**). Moreover, the LH population showed a shift towards higher velocities (**c**). The ranges of these populations are significantly different (**d–f**). Significant difference noted by *
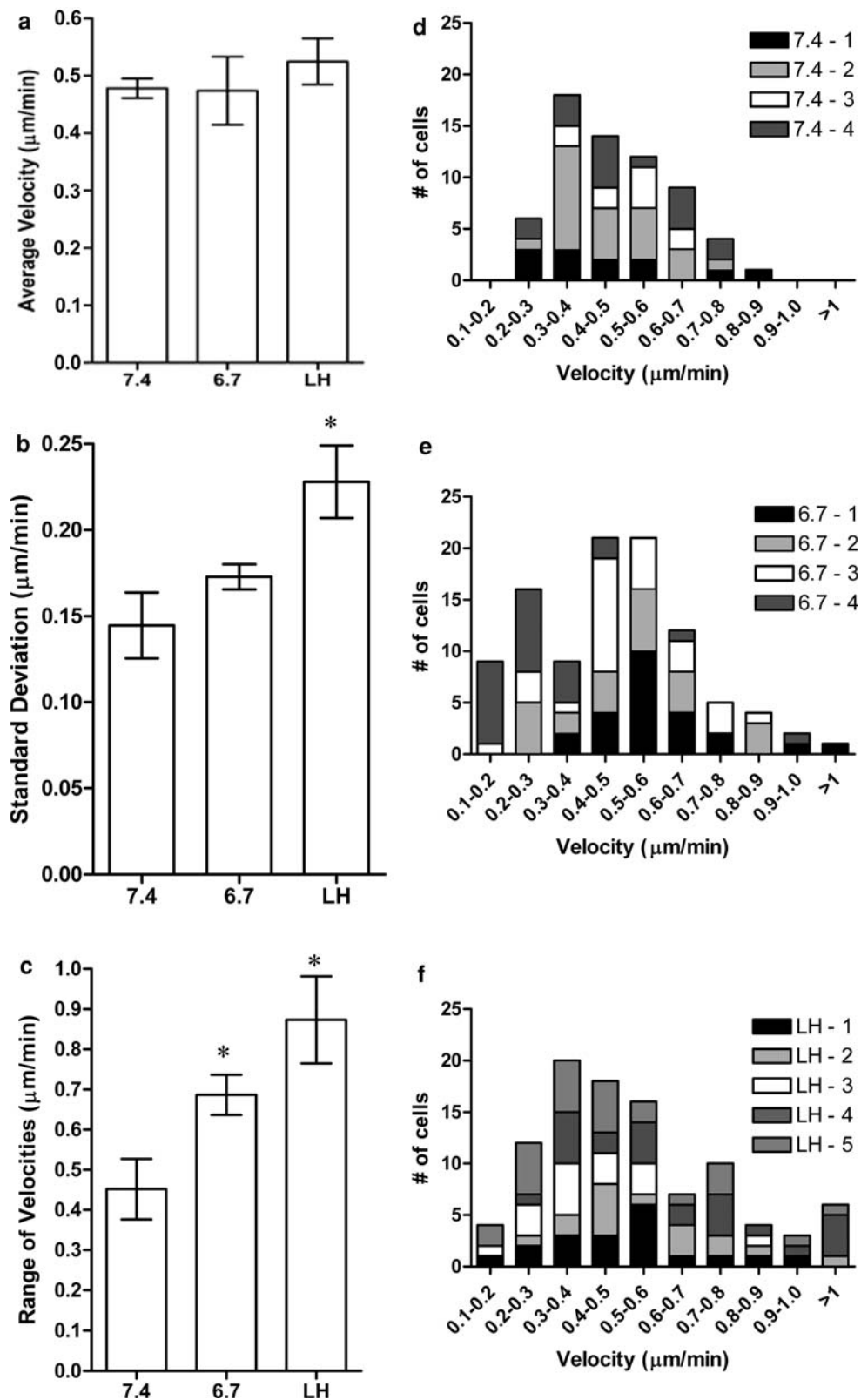
ratio of the LH:7.4 to the 6.7:7.4 data sets. This figure shows the top 500 genes that resulted from an unpaired t-test comparing six slides each. Among the cancer supervised list of 423 genes, the transcriptional repressor SNAI1 showed the highest amount of variance between phenotypes. Among all 44, 059 genes analyzed HEY1, a
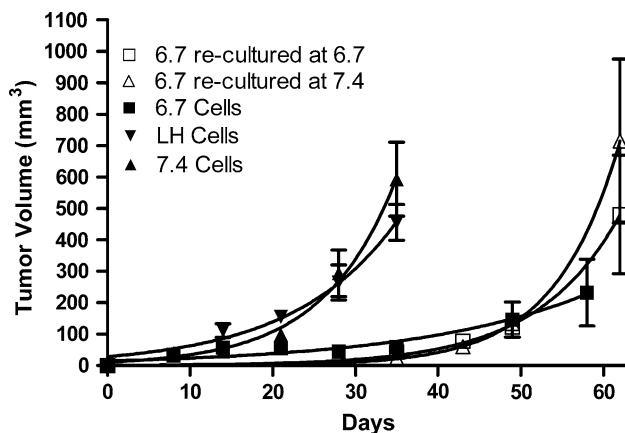
Fig. 6 In vivo tumorigenic assays where cell lines inoculated into flanks of SCID mice show similar growth rates for the C8161/7.4 and /LH phenotypes. The C8161/6.7 phenotype had a significant lag time before tumor growth initiation. Re-culturing of the cells from the C8161/6.7 tumors and re-injection into SCID mice demonstrated that the lag period for growth was maintained in the tumors developed from the recultured cells as well

mediator of Notch signaling, showed the highest variance. Further analysis by quantitative RT-PCR confirmed robust changes in both HEY1 and SNAI1 transcript levels between phenotypes (Fig. 7d). The acid resistant C8161/6.7 phenotype showed only slight differences in RNA levels compared to C8161/7.4 cells. The reacclimated C8161/LH population however, revealed a 4.36 and 11.8 fold increase over the C8161/7.4 expression levels for SNAI1 and HEY1, respectively. This remarkable transcriptional increase in the C8161/LH cells but not the C8161/6.7 phenotype appears mirror the increases observed with in vitro invasion assays and global transcriptional activity.

Figure 8 illustrates the unsupervised and supervised clustering results using hierarchical clustering with Euclidean distance as the similarity measure, where red is overexpressed and green is underexpressed. *Panel a* is the cluster results from 500 random genes; colors at the bottom indicate the three classes of cell treatments. *Panel b* is the dendrogram resulting from the 500 ANOVA genes, showing graphically the dramatic difference in expression between the C8161/6.7 vs. C8161/LH-1 and C8161/6.7 vs. C8161/7.4 data sets, as compared to the C8161/7.4 vs. C8161/LH-1 set. *Panel c* shows 79 cancer genes selected from the 423 cancer genes by filtering for the largest expression change across any of the expression arrays. Again the 7.4/LH comparison showed the greatest difference, recapitulating the dramatic environmental changes these cells have endured through selection and re-acclimation. *Panel d* shows the 40 genes that were common between the ANOVA and the three T-tests. These genes showed an unusually high proportion of ion channel genes, not unsurprising for cells

shifting their physiology to accommodate the lower pH environment.

The Gene Ontology calculation yielded mostly kinase, nucleic acid binding, signal transduction and receptor activity for the cancer gene list [25]. The T-tests and ANOVA results were typified by transferase, catalytic activity, nucleic acid binding, and ion channel activities. The random gene lists identified charperones, translation, and peptidase activities. As mentioned, the 40-gene overlap between ANOVA and T-tests was strongly affected by ion channel functions, but larger lists allowed other functions to be represented. The similarity between the ANOVA and T-test lists and the known cancer list suggests at least some overlap of functions most closely resembling functions consistent with cancer. Pathway analysis yielded similar results, while the cancer gene list identified in addition, Mitogen-activated protein kinase (MAPK), cell cycle, apoptosis, Wnt signaling, and G-protein signaling activities. The T-tests and ANOVA results identified similar functional pathways: inflammation, cell cycle, apoptosis, MAPK and G-protein signaling. Some differences were obvious in these analyses, specifically the abundance of cytokines and inflammation-responsive genes as well as ion channel and receptor activity (data not shown) in greater abundance than the cancer gene results. This highlights some of the lingering adaptive transcriptional changes brought about by the acidic environment. We see that ubiquitous and well-known cancer gene functional groups are recapitulated in the C8161/LH-1 cells, and that C8161/LH-1 cells are different and more transcriptionally active compared to the C8161/6.7 cells grown at pH 6.7.

Discussion

Understanding the relationship between the tumor microenvironment and the events leading to metastasis continues to evolve. This project specifically explored the direct effects of acidosis on melanoma cells by in vitro assays of metastatic potential. Methods were employed allowing quantification of invasion, motility, tumor growth and altered transcription for discrete phenotypes created in an acidic environment. The process of creating these phenotypes along with results from the assays above, support the hypothesis that environmental acidosis selects (rather than induces) a more aggressive phenotype in melanoma.

Data from the real-time invasion assays support the hypothesis that populations acclimated to low pH exhibit higher rates of invasion of a Matrigel™ membrane. Notably, the low pH phenotype cells (C8161/6.7), which was both selected for and maintained at pH 6.7, was not more invasive than the native melanoma cell phenotype (C8161/7.4). This was also observed in the transcriptome
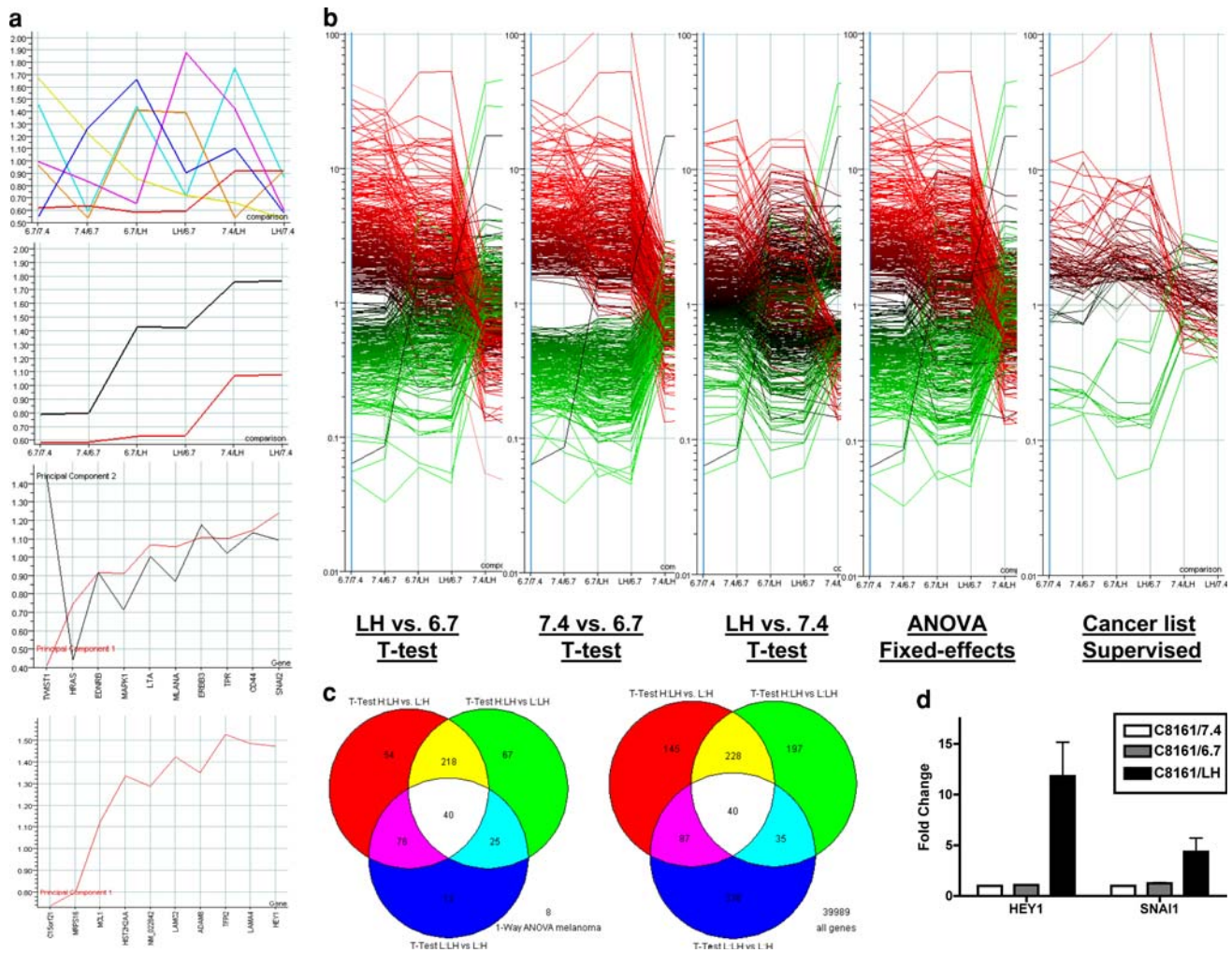
Fig. 7 Expression analysis results. Expression data from 18 separate Agilent Whole Human Genome arrays was analyzed for significance (ANOVA, T-Test) and covariance (Principal Components). (**a**) from top to bottom, show 1, the results from a Principal Components test of all 40,059 genes; 2, the results using only the 500 genes from the ANOVA test; 3, the supervised principal component analysis of ten cancer-specific genes that points to SNAI1 as that gene contributing most to the variance across the three comparisons; and 4, a principal component analysis showing those genes that most significantly differentially expressed overall, pointing to HEY1 as that gene responsible for the most variance across the three comparisons. (**b**) shows all genes that were over- (red) or under- (green) expressed, where the y-axis is the ratio and the x-axis represents each of the six phenotype comparisons, from left to right (Cy5/Cy3): 6.7/7.4, 7.4/6.7, 6.7/LH, LH/6.7, 7.4/LH, LH/7.4. Comparators used common denominators, e.g., 'LH vs. 6.7' compared the LH:7.4 datasets against the 6.7:7.4 datasets, etc. (**c**) Venn diagram showing numbers of significant up- or down-regulated genes in each comparison using a supervised gene list (left panel) and all genes (right panel). (**d**) RT-PCR of HEY1 and SNAI1 expression in C8161/LH and C8161/L cells relative to the parental C8161/7.4 phenotype. Fold-change for each gene was calculated relative to β-Actin transcript levels

results, where changes were most apparent when comparing the C8161/7.4 and C8161/LH-1 phenotypes, despite the fact that these were cultured at the same pH. The elevated invasiveness of the cells selected at low pH only became evident once they were cultured at physiological pH (LH phenotype), which could be interpreted to suggest that although the selection had occurred at low pH, the acidic milieu itself was an inhibitor to invasion. These results were repeated over many months showing the stability of the generated phenotypes, suggesting that the process of acclimation to low pH is a selection event, rather than one of induction. Cells that had merely undergone a transient

shift in gene expression to survive the environment would have reverted back to the phenotypic characteristics of native cells once reintroduced to normal pH. This was not the case, as evidenced by the invasion, motility, morphologic and transcriptomic assays, which all showed that the greatest differences were between the C8161/LH-1 cells and the parental C8161/7.4 cells. The transition from low pH back to normal conditions to form the C8161/LH-1 cells was not accompanied by cell death, as was the original transition from normal to low pH. Instead, the C8161/6.7 cells were capable of surviving both conditions and quickly adapted to the transition. This was also shown in

Table 3 Gene families with significant differences between populations (Gene Ontology)

LH vs 6.7		ANOVA	
Transferase (GO:0016740)	1.23E−08	Transferase (GO:0016740)	2.05E−05
Catalytic activity	2.42E−06	Catalytic activity	0.000297
Nucleic acid binding	0.00551	RNA binding (GO:0003723)	0.00182
Translation factor activity (GO:0008135)	0.00843	Translation factor activity (GO:0008135)	0.00465
Transporter activity	0.00985	Transporter activity	0.0501
Binding	0.0103		
RNA binding (GO:0003723)	0.0132	Cancer genes	
Ion channel activity (GO:0005216)	0.0404	Kinase	1.27E−16
		Protein kinase activity (GO:0004672)	1.27E−16
7.4 vs. 6.7		Catalytic activity	2.29E−15
RNA binding (GO:0003723)	0.000401	Nucleic acid binding	2.55E−09
Transferase (GO:0016740)	0.0017	Binding	4.04E−09
Translation factor activity (GO:0008135)	0.00248	RNA binding (GO:0003723)	2.13E−07
Nucleic acid binding	0.00358	Transcription factor activity (GO:0003700)	1.22E−06
Binding	0.00691	DNA binding	1.34E−06
Catalytic activity	0.0178	Signal transducer activity	2.38E−06
		Receptor activity (GO:0004872)	2.38E−06
LH vs. 7.4		Translation factor activity, (GO:0008135)	2.84E−06
Transferase (GO:0016740)	0.0001	Peptidase activity (GO:0008233)	0.00196
Catalytic activity	0.000297	Hydrolase	0.00376
		Transferase (GO:0016740)	0.00973
		Nucleotide binding (GO:0000166)	0.0109
		Defense immunity protein activity (GO:0003793)	0.0171
		Random genes	
		Chaperone activity (GO:0003754)	0.00016
		Translation factor activity (GO:0008135)	0.00128
		Peptidase activity (GO:0008233)	0.047

the growth curve at pH 7.4, which was acquired immediately upon transferring the C8161/6.7 cells back to normal pH (Fig. 1c). The implication is a stable and transcriptionally-linked accommodation, or new physiological flexibility to new and ionically different environments not seen in the C8161/7.4 cells. However, the increased lag time for tumor growth of the C8161/6.7 cells is inconsistent with this, and may relate to a fragility of these cells, leading to reduced viability upon inoculation.

Since metastasis occurs when a small amount of cells from a primary tumor move to a secondary site, increases in metastatic potential of a few individual cells can be the most important changes in the entire population during cancer progression. For this reason, the motility experiments allowed analyses of individual cells, with surprising results. Although the C8161/6.7 and C8161/LH-1 cells were not different from the C8161/7.4 cells in their average velocity, there was clearly an increase in the heterogeneity of phenotypes in these two treated populations. Both the C8161/6.7 and C8161/LH-1 cells showed significantly greater ranges and standard deviation values with respect to

velocity distributions in a given field. In other words, both faster and slower cells were present in the treated cells compared to untreated populations. The observation of stressful environments increasing phenotypic and genomic heterogeneity is well known among prokaryotes, thus, the increased heterogeneity among the C8161/6.7 cells was expected. It was surprising that this phenotypic heterogeneity was maintained after switching cells back to the normal pH, but was further evidence that some C8161/LH-1 cells are permanently more motile and invasive after low pH selection compared to untreated cells. The continued heterogeneity reinforces the notion that the acidic media selected for an array of adaptable phenotypes that remain competitive within the LH-1 population even after the environmental stress is alleviated. The discrete transcriptional changes found in the C8161/LH-1 cells correlate well to increased invasive and adaptive potential. For example, the BioCarta, GenMapp and KeGG database analyses all identified significant changes in the expression of metalloproteinase and cell adhesion genes, which are positively linked with metastatic transition via degradation

Table 4 Genes with significantly altered expression

| LH vs. 6.7			ANOVA		
BioCarta	GenMapp	KeGG	BioCarta	GenMapp	KeGG
Peroxisome	Translation fact.	MapK	PPARa	Inflammation	MAPK
TNFR1 Signal	Inflammation	Complement	Inflammation	Apoptosis	Complement
B cell survival	Apoptosis	Apoptosis	TNFR1	Metalloproteinase	Cell Cycle
Inflammation	Metalloproteinase	Wnt Signaling	Cytokines	Wnt	Apoptosis
7.4 vs 6.7			Cancer genes		
BioCarta	GenMapp	KeGG	BioCarta	GenMapp	KeGG
Cell Cycle	Inflammation	Cell Cycle	MAPKinase	Wnt Signalling	MaPK
Inflammation	Wnt Signaling	MAPK	Cell Cycle	Apoptosis	Cell Cycle
TNFR1 Signal	MAPK	Wnt Signaling	G1 to S	MapK Cascade	Wnt Signaling
FAS Signal	Apoptosis	Apoptosis	IL-2 Receptor	G-Protein Signaling	Cell Adhesion
LH vs 7.4			Random genes		
BioCarta	GenMapp	KeGG	BioCarta	GenMapp	KeGG
PPARa	Metalloproteinase	MAPK	Cortisteroids	Translation	Ribosome
Inflammation	Inflammation	Cell cycle	Hypoxia in heart	Wnt signaling	Ubiquitin
Cytokine	Apoptosis	Ribosome	Oocyte maturat.	G-protein signaling	Cholera infection
Adhesion	G-protein	Apoptosis	mCalpain	Inflammation	Prion disease
			Peroxisome	Infertility	Huntington's
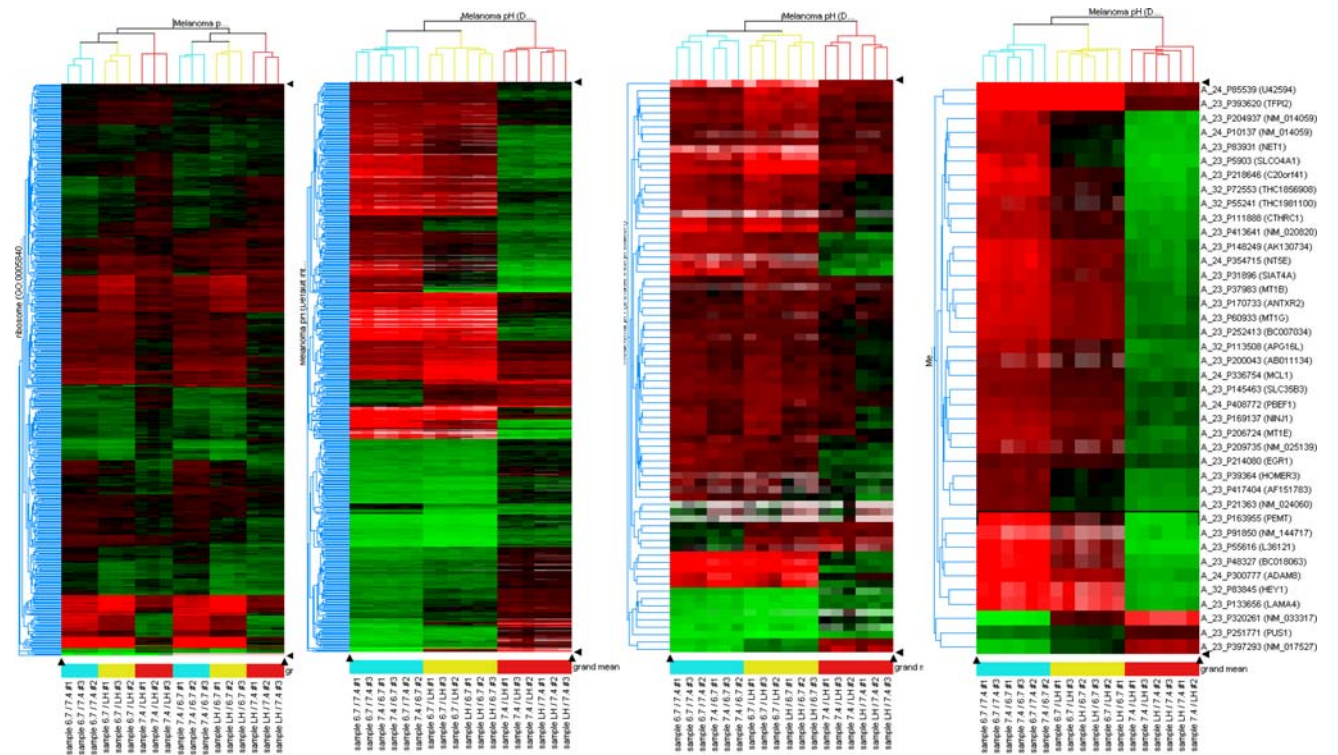
Fig. 8 Hierarchical clustering of four sets of genes using Euclidean distance as the similarity measure. The X-axis indicates the ratio comparisons clustered in three sets: 6.7–7.4; LH to 6.7 and LH to 7.4. As in Fig. 6, numerators were Cy5 and denominators were Cy 3 labeled. (**a**) is a quality control clustering of a random set of 500 genes showing a lack of grouping. (**b**) shows the results from the 500 ANOVA genes with the strongest differences seen between the pH 7.4/LH group and all others. (**c**) shows effects on 79 cancer-specific genes including hypoxia, signal transduction, and vascularization genes, again recapitulating the general pattern of distinction. (**d**) is a dendrogram showing the 40 genes that are common between the ANOVA and the three T-test gene lists

of the basement membrane and increased motility (Table 4). Notably, these functions were not found to be overexpressed when comparing C8161/6.7 cells with the parental C8161/7.4 cells. This result parallels our phenotypic results where the C8161/LH-1 population showed increased invasiveness and the C8161/6.7 cells did not.

The observed changes in expression also reveal functional similarity to those seen in cells under hypoxic stress. Although microenvironmental acidosis is often regarded as a consequence of hypoxia brought about by signaling through HIF-1α and increased glycolosis, the C8161/LH-1 cells appear to harbor some of these changes directly. The two genes found to be most overexpressed in the C8161/LH-1 line were HEY1 and SNAI1, both of which are transcriptional repressors directly activated by HIF-1α signaling. The link between hypoxia and Notch signaling has become increasingly indicated to promote proliferation, adaptability and survival among tumor populations [26]. Moreover, SNAI1, is a direct target of HIF-1α and is correlated to metastasis through promotion of MMP expression and the epithelial-to-mesenchymal transition [27–29]. Taken together with the functional group changes found in the database analysis, these results support the notion that many of the changes linked with hypoxic stress are also triggered during acidosis. Furthermore, it appears that activation of these pathways is in part responsible for the stable phenotypic heterogeneity and adaptability seen in the C8161/6.7 and C8161/LH-1 populations.

In summary, significant cell mortality during acclimation to low pH, and morphological differences support the hypothesis that acidic selection of melanoma cells generates discrete new phenotypes, one of which exhibits a robust increase in invasive potential when re-acclimated to normal pH. This study specifically focused on the effects of acidic selection in an invasive melanoma cell line, however the generality of this phenomenon is being explored in a panel of human cancers with similar results. For example, MDA-MB-231 breast cancer cells exhibit the same selection kinetics and produce low pH (MDA-MB-231/6.7) and re-acclimated (MDA-MB-231/LH-1) populations with comparable invasive properties to those seen in melanoma (Supplemental Figure 1). In the context of in vivo cancer progression, we can assume that the most acidic microenvironments are those furthest from blood vessels [6, 30] and that these occur in the lumens of ducts [31]. Selection under these conditions leads to cells that survive and exhibit phenotypic heterogeneity, evidenced by a large range of motilities. Eventually, some of the more motile cells will find themselves near the basement membranes, which are close to the underlying blood vessels and are expected to be at or near neutral pH. Once in this environment, the selected cells are more invasive and are thus more capable of metastasis. The mechanisms underlying this transition are not yet understood.

References

1. Bernards R, Weinberg RA (2002) A progression puzzle. Nature 418:823–823
2. Yun Z, Giaccia AJ (2003) Tumor deprivation of oxygen and tumor suppressor gene function. Method Mol Biol 223:485–504
3. Koumenis C, Alarcon R, Hammond E et al (2001) Regulation of p53 by hypoxia: dissociation of transcriptional repression and apoptosis from p53-dependent transactivation. Mol & Cell Biol 21:1297–1310
4. Yasuda S (1995) Hexokinase II and VEGF expression in liver tumors: correlation with hypoxia-inducible factor 1 and its significance. Proc Natl Acad Sci USA 92:5965–5968
5. Czernin J, Phelps ME (2002) Positron emission tomography scanning: current and future applications. Ann Rev Med 53:89–112
6. Schornack PA, Gillies RJ (2003) Contributions of cell metabolism and H + diffusion to the acidic pH of tumors. Neoplasia (New York) 5:135–145
7. Gillies RJ, Raghunand N, Karczmar G et al (2002) MR Imaging of the tumor microenvironment. J Magn Reson Imaging 16:430–450
8. Park H, Lyons JC, Ohtsubo T et al (1999) Acidic environment leads to p53 dependent induction of apoptosis in human adenoma and carcinoma cell lines: implications for clonal selection during colorectal carcinogenesis. Oncogene 18:3199–3204
9. Williams AC, Collard TJ, Paraskeva C (1999) An acidic environment leads to p53 dependent induction of apoptosis in human adenoma and carcinoma cell lines: implications for clonal selection during colorectal carcinogenesis. Oncogene 18:3199–3204
10. Shrode LD, Tapper H, Grinstein S (1997) Role of intracellular pH in proliferation, transformation, and apoptosis. J Bioenerg Biomembr 29:393–399
11. Park HJ, Lyons JC, Ohtsubo T et al (1999) Acidic environment causes apoptosis by increasing caspase activity. Br J Cancer 80:1892–1897
12. Gatenby RA, Gawlinski ET (1996) A reaction-diffusion model of cancer invasion. Cancer Res 56:5745–5753
13. Rozhin J, Sameni M, Ziegler G et al (1994) Pericellular pH affects distribution and secretion of cathepsin B in Malignant Cells. Cancer Res 54:6517–6525
14. Sounni NE, Noel A (2005) Membrane-Type Matrix Metalloproteinases and Tumor Progression. Biochimie 87:329–342
15. Martinez-Zaguilan R, Seftor EA, Seftor RE et al (1996) Acidic pH enhances the invasive behavior of human melanoma cells. Clin Exp Metastasis 14:176–186
16. Rochefort H, Chalbos D, Cunat S et al (2001) Estrogen regulated proteases and antiproteases in ovarian and breast cancer cells. J Steroid Biochem Mol Biol 76:119–124
17. Ferrier CM, van Muijen GNP, Song CW (1998) Proteases in cutaneous melanoma. Ann Med 30:431–442
18. Goretzki L (1992) Effective activation of the proenzyme for of the urokinase-type plasminogen activator (pro-uPA) by the cysteine protease cathepsin L. FEBS Lett 297:112–118

19. Hanahan D, Weinberg RA (2000) The hallmarks of cancer. [Review] [94 refs]. Cell 100:57–70

20. Schlappack OK, Zimmermann A, Hill RP (1991) Glucose starvation and acidosis: effect on experimental metastatic potential, DNA content and MTX resistance of murine tumour cells. Br J Cancer 64:663–670

21. Webb SD, Sherratt JA, Fish RG (1999) Alterations in proteolytic acitivity at low pH and its association with invasion: a theoretical model. Clin Exp Metastasis 17:397–407

22. Rofstad EK, Mathiesen B, Kindem K et al (2006) Acidic extracellular pH promotes experimental metastasis of human melanoma cells in athymic nude mice. Cancer Res 66:6699–6707

23. Krishnamurty C, Rodriguez J, Raghunand N et al (2005) Automatic Lesion tracking in echo-planar diffusion weighted liver MRI: an active countour based approach. Proc Int Soc Magn Reson Med 13:1889

24. Wolber PK, Whannon KW, Fulmer-Smentek SB et al (2002) Robust local normalization of gene expression microarray data. Agilent Technical Note 1015:1–4

25. Khatri P, Draghici S, Ostermeier GC et al (2002) Profiling Gene Expression Utilizing Onto-express. Genomics 79:266–270

26. Diez H, Fischer A, Winkler A et al (2007) Hypoxia-mediated activation of Dll4-Notch-Hey2 signaling in endothelial progenitor cells and adoption of arterial cell fate. Exp Cell Res 313:1–9

27. Barbera MJ, Puig I, Dominguez D et al (2004) Regulation of Snail transcription during epithelial to mesenchymal transition of tumor cells. Oncogene 23:7345–7354

28. Imai T, Horiuchi A, Wang C et al (2003) Hypoxia attenuates the expression of E-cadherin via up-regulation of SNAIL in ovarian carcinoma cells. Am J Pathol 163:1437–1447

29. Miyoshi A, Kitajima Y, Sumi K et al (2004) Snail and SIP1 increase cancer invasion by upregulating MMP family in hepatocellular carcinoma cells. Br J Cancer 90:1265–1273

30. Helmlinger G, Yuan F, Dellian M et al (1997) Interstitial pH and pO2 gradients in solid tumors in vivo: high-resolution measurements reveal a lack of correlation. Nat Med 3:177–182

31. Gatenby RA, Gillies RJ (2004) Why do cancers have high aerobic glycolysis? Nat Rev Cancer 4:891–899